Received: 30 August 2021 | Revised: 24 April 2022 | Accepted: 27 May 2022

DOI: 10.1049/smt2.12112

IET Science, Measurement & Technology

The Institution of Engineering and Technology WILEY

ORIGINAL RESEARCH

Simulation of a non-linear, time-variant circuit using the Haar wavelet transform

Georgios G. Roumeliotis | Jan Desmet | Jos Knockaert

Department of Electromechanical, Systems, and Metal Engineering, Faculty of Engineering and Architecture, Ghent University, Research Group EELab/Lemcko, Kortrijk, Belgium

Correspondence
Georgios G. Roumeliotis, Department of Electromechanical, Systems and Metal Engineering, Faculty of Engineering and Architecture, Ghent University, Research Group EELab/Lemcko, Sint-Martens-Latemlaan 2B, 8500 Kortrijk, Belgium.
Email: Georgios.Roumeliotis@UGent.be

Abstract

Wavelet theory has disentangled numerous complexities, including those pertinent to transient and steady-state responses of systems, when Laplace and Fourier transforms face insoluble obstacles. Reactive linear components (e.g. inductors and capacitors) are typically handled in the frequency plane. Non-linear (e.g. diodes) or time-variant components (e.g. switches) are conventionally simulated in the time plane (e.g. a diode via its I–V characteristic) and are considered open or short circuits in AC analyses (e.g. in circuit simulation software). Although translating circuits in an alternative plane, such as the Haar wavelet plane, significantly simplifies the process, a wide integration of wavelets into instruments and education is not yet realised; an underlying reason is the considerate complexity of applying wavelet theory to circuits and signals. The aim of this paper is to bridge this gap, providing a new user-friendly, Laplace-alike approach, utilising measurement-based models and the Haar wavelet. The Haar wavelet transform and a numerical method for the inverse Laplace transform which uses the Haar operational matrix are applied, to calculate the total current of a non-linear, time-variant system, that is the total current of a voltage source which powers a non-linear, time-variant load.

1 | INTRODUCTION

The Fourier transform, its discrete time equivalent, the discrete Fourier transform and the fast Fourier transform (FFT) algorithm have long been indispensable tools for science and engineering. Since the conception of the FFT by Carl Friedrich Gauss in 1805 and Jean Baptiste Joseph Fourier in 1822, as described in a history report regarding the FFT by Heideman et al. [1], they have been widely used to simplify differential equations. Two of the most common applications are the steady-state spectrum of output signals and the impedance of linear, time-invariant (LTI) circuits. The Laplace transform, as a generalisation of the Fourier transform, is used to additionally incorporate the transient state of outputs and systems. In reality, however, no system exists that is either linear or time-invariant. Macroscopically, all materials are slowly advancing towards a thermodynamic equilibrium, deteriorating with time. Moreover, all systems have a wide span of variables that affect them such as temperature, mechanical stress and electromagnetic fields. A system can only resemble an LTI system.

Often a non-linear behaviour of a system becomes too significant to disregard. Simplifications such as the small signal approximation in amplifiers theory are often useful, because the Fourier and Laplace transforms cannot typically be applied if a non-linear equation is needed to describe the system.

When a system is time-variant (e.g. switched capacitor), the differential equations needed to describe it are too difficult to handle in the time plane. Transformation to the s-plane offers a solution to a limited extent, as the inverse Laplace of such a system usually becomes too intricate to solve and only numerical methods can be used to determine its output.

Since its inception by Alfréd Haar in 1909, wavelet theory has been invaluable in physics (e.g. used for transmission line theory in lumped and distributed-parameter systems by Chen and Hsiao [2]) but also in various aspects of technology with applications such as groundbreaking compression algorithms as reported by Jain and Pankanti [3] to identify fingerprints automatically, in an attempt to compress and scan through the overwhelming fingerprints database of the Federal Bureau of Investigation (USA). The Haar wavelet has moreover been used to calculate the inverse Laplace transform as conceptualised by Wu et al. [4], various examples of which are also shown by Aznam et al. [5]. Furthermore, it has been proven to efficiently handle non-linear circuit analysis as shown by Ohkubo et al. [6], Nakabayashi et al. [7], Sliwinski [8] and even time-variant systems as shown by Hsiao et al. [9–11]. It is noted that even though the Haar wavelet possesses many favourable properties, mainly based on its binary 0–1 simplicity being a square wave, research on wavelets also includes other wavelet types. The fast wavelet collocation method, as presented by Zhou and Chen [12, 13], can be applied in a variety of wavelet types, one of the most common wavelets being the Walsh wavelet as shown in Ref. [14], and delivers comparable results to the more common Fourier transform, as reported by Strang [15]. The aforementioned key publications span several decades and are indicative of the progress velocity in this field of research. Even though being an important tool for science, engineering and technology, the initial complexity of using it for practical applications can possibly explain the reluctance of it, replacing or overwhelming the conventional methods for circuit analysis such as the Fourier and Laplace transforms. It is notable that due to the nature of the methods involving wavelet transforms, which handle a variety of matrices and vectors, even a small mistake, such a wrong index, is enough to cause a completely erratic calculation. This can be caused either by wrong or unambiguous descriptions (e.g. not defining exactly all variables and symbols).

A methodology is presented, using the Haar wavelet, which can be applied not only in linear but also in both non-linear and time-variant systems. It utilises the same principles as the Laplace transform in the case of impedance and additionally applies to common non-linear and time-variant components. The Haar wavelet transform is effectively masked and presented in such a way that it seemingly resembles the Laplace transform which is the norm in the case of combining reactive linear components and sinusoidal signals. This way, the process of utilising the benefits of the Haar wavelet becomes significantly uncomplicated, as almost all principles of the Laplace transform of linear components can be utilised. Moreover, load modelling using direct measurements is performed in order to demonstrate all the steps from measurement up to simulation for non-linear components such as diodes. Consequently, it demonstrates a way in which education and also scientific instruments, such as network analysers, could advance from the LTI theory to a more generalised concept, by accurately including non-linear and time-variant elements.

The presented step-by-step approach provides an essential connection between measurements and simulation. It presents the scenario of simulating a circuit which includes components the user has previously measured and modelled, as is the case in this work. Specifically, a switched user-defined diode in parallel with a user-defined linear load are powered by a voltage source. Current–voltage and impedance measurement-based models are created in order to showcase the possibility of creating and simulating user-defined models. Three versions of this circuit are simulated, using different diodes. First, direct measurements

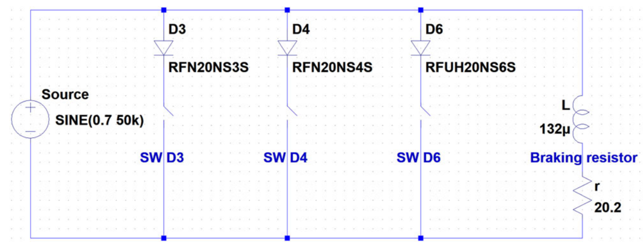

FIGURE 1 The circuit simulated using the Haar wavelet transform

on diodes and a linear load are performed in order to investigate their exact properties. Second, their characteristics are modelled. Third, the input and all modelled characteristics are combined in the Haar plane in the hypothetical scenario of each diode being in series with an ideal switch (Figure 1). Finally, the inverse Haar transform is performed to calculate the output of the system; in this case, the total current of the ideal voltage source. In theory, a voltage source will always have a series impedance. In the presented example, however, as the source represents a hypothetical voltage measurement at the input of a load, and not an actual voltage source, a series impedance is not necessary. The usefulness and simplicity of this approach in load modelling are showcased, effectively circumventing the intricacies of forward and inverse linear transforms of non-linear, time-variant systems. The state of the art for the most part consists of various theoretical concepts and potential applications, but wide range implementation in commercial products (e.g. network analysers and oscilloscopes) or education remains yet a slowly progressing aspect. Indicative recent advances are in applications such as digital audio signal processing [16], reactive elements circuit analysis [17], time-variant circuits [18, 19], fault detection in linear circuits [20] and promising theoretical analyses such as the work by Ratas et al. [21] for solving non-linear boundary values. Finally, a more complete summary of wavelet types and transforms as well as modern concepts and applications can be found in works such as the book by Akujuobi [22].

2 | METHODS

2.1 | Haar wavelet matrices and vectors

The key element in the use of the Haar wavelet and its operational matrix, the Haar wavelet matrix (H), is that it only needs to be calculated once, as shown in Ref. [5], or loaded from a pre-existing library. Even though the calculation of H is time-consuming for a processor, the time for loading it from a library is insignificant. For example, calculating a 1024×1024 H matrix (e.g. on PTC Mathcad) takes hours, but loading it from a data file and using it in calculations such as matrix multiplication or summation takes only a fraction of a second. It is noted that the number of time points used (N) for the representation of a time signal determines the dimensions of the $N \times N$ square matrix H. All forward and inversion operations can then use this matrix, significantly reducing the calculation process time as compared to solving a system in the time plane using integrals and differential equations. Depending on the size of N and the time length of the simulation (τ), assuming that it starts on $t_0 = 0$, the block pulse operational matrix (F) and the generalised Haar operational matrix (Q) are defined. The exact same definitions for H, F and Q as in Ref. [5] are used. For $N = 4$ and $\tau = 1$, the matrices H, F, Q and the corresponding time vector (t) are as follows:

$$H = \begin{bmatrix} 1/2 & 1/2 & 1/2 & 1/2 \\ 1/2 & 1/2 & -1/2 & -1/2 \\ 1/\sqrt{2} & -1/\sqrt{2} & 0 & 0 \\ 0 & 0 & 1/\sqrt{2} & -1/\sqrt{2} \end{bmatrix}, \tag{1}$$

$$F = \frac{\tau}{8} \cdot \begin{bmatrix} 1 & 2 & 2 & 2 \\ 0 & 1 & 2 & 2 \\ 0 & 0 & 1 & 2 \\ 0 & 0 & 0 & 1 \end{bmatrix}, \tag{2}$$

$$Q = \begin{bmatrix} 1/2 & -1/4 & -1/\left(8\sqrt{2}\right) & -1/\left(8\sqrt{2}\right) \\ 1/4 & 0 & -1/\left(8\sqrt{2}\right) & 1/\left(8\sqrt{2}\right) \\ 1/\left(8\sqrt{2}\right) & 1/\left(8\sqrt{2}\right) & 0 & 0 \\ 1/\left(8\sqrt{2}\right) & -1/\left(8\sqrt{2}\right) & 0 & 0 \end{bmatrix} \tag{3}$$

and

$$t = \begin{bmatrix} 0 \\ 0.25 \\ 0.5 \\ 0.75 \end{bmatrix}. \tag{4}$$

Any forward (V_H) or inverse Haar wavelet transform (V_{IH}) of a given vector $\boldsymbol{V}$ is conveniently performed by the following equations:

$$V_H = H \cdot V \tag{5}$$

and

$$V_I H = H^{(-1)} \cdot V. \tag{6}$$

In order to benefit from the useful properties and logic of the Laplace transform for linear components, which uses the variable s, a similar variable matrix (S) is created which is the inverse of Q. For $N = 4$ and $\tau = 1$ it is

$$S = Q^{-1} = \begin{bmatrix} 0 & 0 & 4 \cdot \sqrt{2} & 4 \cdot \sqrt{2} \\ 0 & 0 & 4 \cdot \sqrt{2} & -4 \cdot \sqrt{2} \\ -4 \cdot \sqrt{2} & -4 \cdot \sqrt{2} & 16 & 32 \\ -4 \cdot \sqrt{2} & 4 \cdot \sqrt{2} & 0 & 16 \end{bmatrix}. \tag{7}$$

This matrix can be conveniently used to represent the impedance of an inductor (Z_L) or a capacitor (Z_C) as

$$Z_L = S \cdot L \tag{8}$$

and

$$Z_C = \frac{1}{S \cdot C} \tag{9}$$

where L and C are the values of the inductor and capacitor, respectively. The impedance of a resistor (Z_R) uses the identity matrix I_m as it is invariant of S. For $N = 4$ and a resistor of value R,

$$I_m = \begin{bmatrix} 1 & 0 & 0 & 0 \\ 0 & 1 & 0 & 0 \\ 0 & 0 & 1 & 0 \\ 0 & 0 & 0 & 1 \end{bmatrix} \tag{10}$$

and

$$Z_R = I_m \cdot R. \tag{11}$$

The resistance of a time-variant load (R_D), such as a resistor whose value is time-variant, can also be represented by a Haar plane impedance matrix [6], by converting the vector into a diagonal square matrix. It is noted that an impedance matrix in this context does not have to simulate a linear component, that is even though the property of impedance can only be defined for linear components, other non-linear or time-variant components can still be represented by what is denoted here as an impedance matrix. This characterisation is given here only to resemble the concept of impedance, in the context of using this matrix in the Haar plane, in a similar way to how the impedance of a linear component would be handled in the Laplace plane. For $N = 4$ and a vector $\boldsymbol{r}$ which defines the value of the resistance in every time point,

$$r = \begin{bmatrix} R_0 \\ R_1 \\ R_2 \\ R_3 \end{bmatrix} \tag{12}$$

$$\text{diag}\ (r) = \begin{bmatrix} R_0 & 0 & 0 & 0 \\ 0 & R_1 & 0 & 0 \\ 0 & 0 & R_2 & 0 \\ 0 & 0 & 0 & R_3 \end{bmatrix} \tag{13}$$

and

$$r_d = H \cdot \text{diag}\,(r) \cdot H^T \tag{14}$$

where T denotes matrix transposition. The matrix created by Equation (14) can also be used to approximate the resistance of a non-linear component such as a diode or a switch by defining their resistance at each time point, as performed on Ref. [6]. In this case, as the voltage is known at the terminals of each diode, the I–V of each diode can be used to calculate its resistance at each time point (as shown in Section 2.4).

2.2 | A simulated circuit using measurement-based models

In order to demonstrate the simulation described earlier, the schematic shown in Figure 1 is simulated. The necessary properties of a braking resistor and three diodes were defined using direct measurements and then modelled. The braking resistor is a 20-kW, 20-**Ω** resistance (article reference 6SE7023-2ES87-2DC0). The diodes used are an ROHM RFN20NS3S (D3), an ROHM RFN20NS4S (D4) and an ROHM RFN20NS6S (D6).

The simulated circuit consists of a sinusoidal voltage source, three switched power diodes which act as non-linear time-variant loads and a braking resistor which acts as a linear impedance load. The combination of the analogue signal of the voltage source with the ON/OFF digital signals which direct the switches results in a mixed signal circuit. The source has an amplitude of 0.7 V and a frequency of 50 kHz (f_s). All of the diodes have a maximum rms rating of 20 A. The manufacturer states a threshold voltage range of 1.1 to 1.35 V for D3, 1.3 to 1.55 V for D4 and 1.25 to 1.55 V for D6. The aim of comparing different diodes is to show the current differences when applying different non-linear loads and whether a difference between the datasheets and measurements can be noticed or not and consequently creating a user-defined instead of a pre-existing model. As a diode is not time-variant in principle, to make the total load that the voltage source feeds time-variant, a switching scheme is created. The simulated switches are automatically operated, having only one diode switched per case examined, whereas all other switches remain off.

2.3 | Impedance measurement and modelling of the braking resistor

On the braking resistor, first impedance measurements were conducted in order to additionally create a realistic user-defined linear load. The impedance measurements performed using a

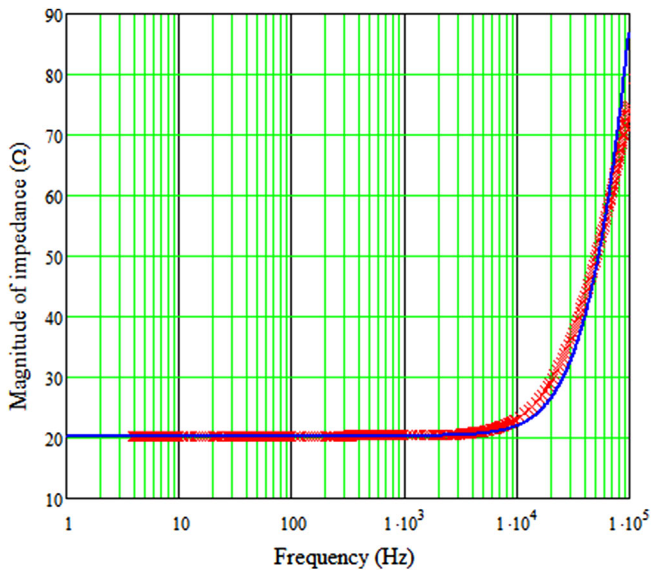

FIGURE 2 Impedance magnitude measurement (red) and fitting (blue) for the braking resistor

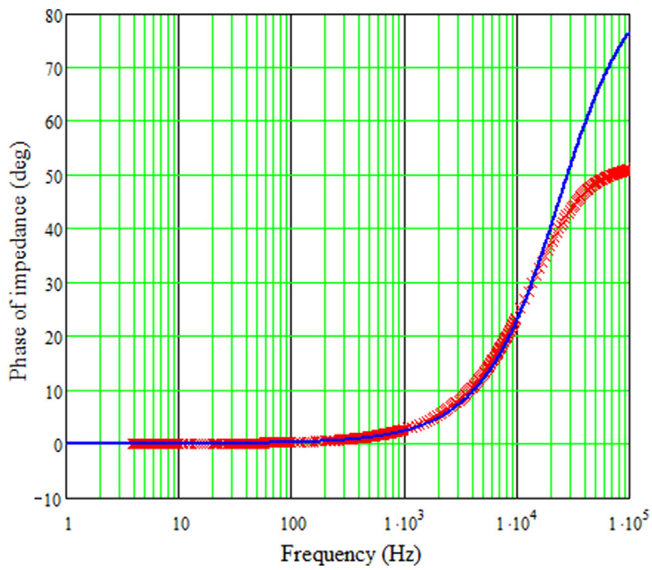

FIGURE 3 Impedance phase measurement (red) and fitting (blue) for the braking resistor

Hioki IM3536 LCR instrument are shown in Figure 2. A setting of 1 V_{AC} (rms) was used for this frequency sweep. Thermal stability was assured, as this voltage was not large enough to noticeably change the temperature of the load. It is noted that the braking resistor has heat sinks incorporated in its structure. Subsequently, the impedance of the braking resistor was simulated using a resistor of value $r_b = 20.2\ \Omega$ in series with an inductor of value $L_b = 132\ \mu\text{H}$, as shown in Figure 1, in order to model the impedance measurement. The impedance magnitude and phase measurements as well as their respective fitting curves are shown in Figures 2 and 3.

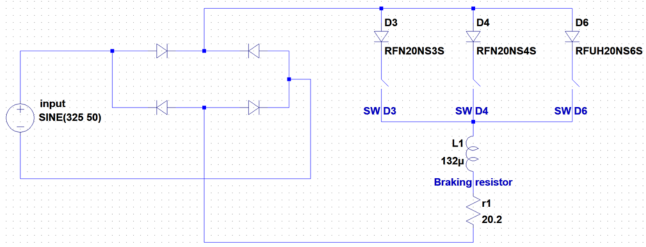

FIGURE 4 The circuit used in order to obtain the *I–V* measurements for D3, D4 and D6

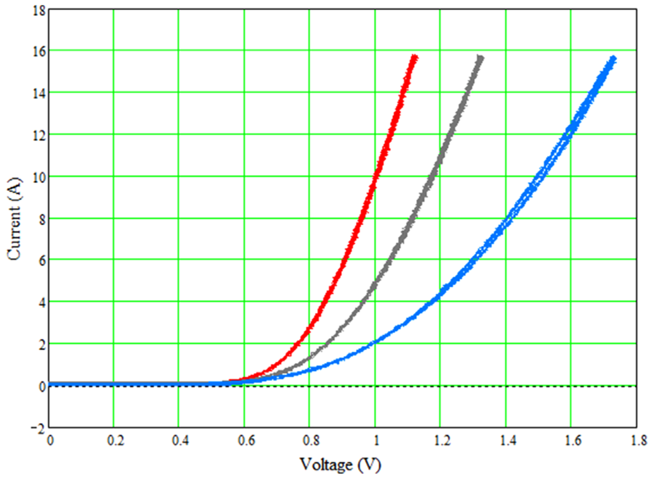

FIGURE 5 *I–V* measurements of diodes D3 (red), D4 (grey) and D6 (blue). 'Dual line' visible in D6 measurement as an effect of temperature

Second, using the LCR instrument in 1 V_{DC}, the same value of 20.2 Ω was confirmed for 0 Hz (DC). This measurement was performed in order to verify its DC resistance.

Third, an additional impedance test measurement on the braking resistor was performed in order to verify its linearity at higher voltages and potentially temperatures. The network voltage was used as a source which can provide high currents, nominally 230-V_{AC} rms, 50 Hz, maximum 16-A rms. The network voltage was measured with a FLUKE 117 multimeter. Finally, using a Tektronix TCP305A current probe, powered by an ROHDE and SCHWARZ RT-ZA13 power supply, the current was measured. Dividing rms voltage by rms current, the same value of 20.2 Ω was confirmed. Thermal stability here was assured by the fact that the time needed for this measurement was only 1 s approximately. The calculated value of 20.2 Ω is in agreement with the impedance measurement of the LCR at 50 Hz.

Comparing the results of the three measurements, the stability and thus the linearity of the impedance of the braking resistor is indicated, in the range of 1 V (LCR voltage amplitude) to 325 V (network voltage amplitude) and 0–300 Hz. This comparison was performed as a precautionary test in order to exclude a highly non-linear load which would contradict its use as a linear load and to linearly adjust the current of the *I–V* measurements, as explained in Section 2.4. Other resistive loads, including incandescent lamps, were rejected as this comparison method proved them to be non-linear; their non-linearity, having different resistance at 50 Hz when comparing between 1 V_{AC} (LCR at 50 Hz) and 230 V_{AC} (network voltage), is assumed to mainly have been an effect of their rapidly increasing temperature.

2.4 | *I–V* measurements and modelling of the power diodes

A second circuit incorporating the aforementioned components was manufactured, in order to measure the characteristics of the diodes and the braking resistor. On the three diodes, current–voltage (*I–V*) measurements on forward bias were performed. The *I–V*s were obtained by using the components in a configuration as shown in Figure 4. It is noted that this configuration was used only for the *I–V* measurements, and it is not the simulated circuit that was previously shown in Figure 1. For each *I–V*, the switch of the diode under test was manually closed, whereas the others remained open.

The network voltage was used as a voltage source which can provide high currents. The braking resistor was put in series with one diode at a time in order to linearly reduce the forward bias current. A bridge MB3510 rectifier was inserted to eliminate the high negative voltages that would otherwise occur in reverse bias. This technique allowed a higher accuracy measurement of the small forward bias voltage drop on the diodes as it could be directly measured without the need of an attenuation probe. Furthermore, a heat sink was attached to the bridge rectifier and the diodes under test. The voltage drop of each diode was measured on Channel 1 of a battery-powered oscilloscope (PicoScope 5244B). The voltage across the braking resistor was accessed by a Pico TA057 voltage battery-powered differential probe at a 200× attenuation setting. The output of the differential probe was measured on Channel 2 of the oscilloscope. For a time duration of 50 ms, the continuous voltage measurements of both channels were captured. The linear impedance of the braking resistor, verified to be 20.2 Ω, enabled converting its voltage drop into current. Using this technique, all *I–V*s of the three diodes were obtained, shown in Figure 5.

An additional effort for the thermal stability of the diodes was made, the *I–V* measurement lasting less than 1 s. Nevertheless, some thermal instability is evident in the measurement of D6 in Figure 5. It has an apparent 'dual line' form; of the two visible blue lines, the left one is at a lower temperature as the threshold voltage in diodes rises with temperature elevation.

The *I–V*s were then custom fitted for the range 0–0.8 V, using the following equation:

$$I = m \cdot V^{p}. \tag{15}$$

The respective m and p factors are shown in Table 1 and the fitted curves in Figure 6.

Using the *I–V* measurements, the non-linear resistance of each diode (R_{D3}, R_{D4}, R_{D6}) as a function of voltage was calculated as voltage divided by current and is shown in Figure 7.

TABLE 1 The diodes fitting parameters

Diode	*M*	*p*
D3	15.9	7.81
D4	5.60	6.56
D6	2.16	5.02

TABLE 2 Extra parameters of the simulated circuit

Parameter	Value
$R_{3\,reverse}$	7.0 GΩ
$R_{4\,reverse}$	8.6 GΩ
$R_{6\,reverse}$	12.0 GΩ
R_{on}	0 Ω
R_{off}	1 TΩ
f_{sw}	100 kHz

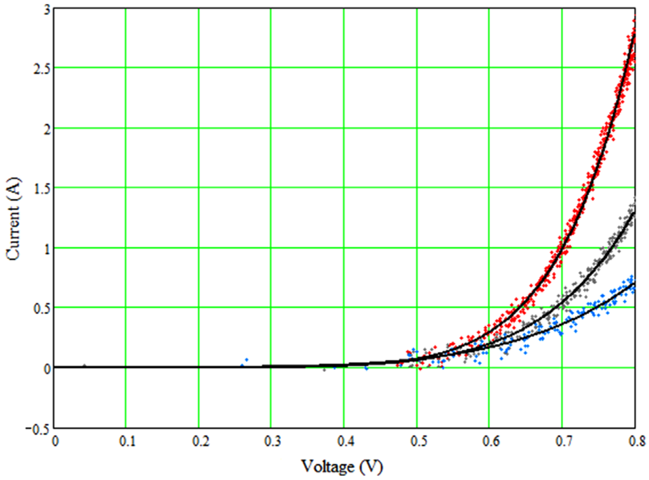

FIGURE 6 *I–V* measurements of diodes D3 (red), D4 (grey) and D6 (blue) and their respective fitting curves in the range 0–0.8 V

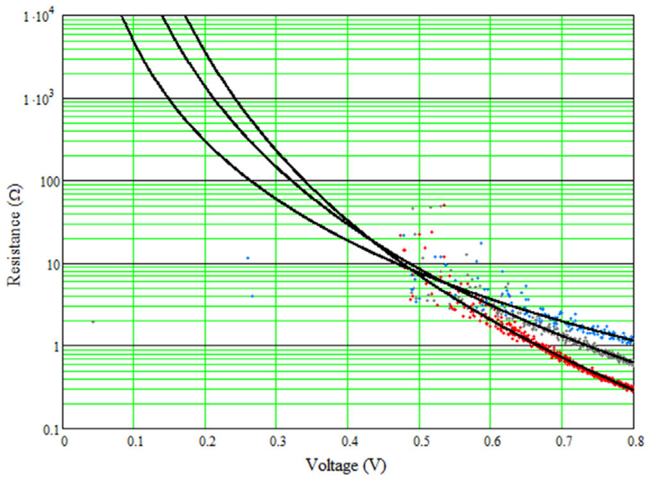

FIGURE 7 Resistance of diodes D3 (red), D4 (grey) and D6 (blue) as calculated using the direct *I–V* data, and their respective fitted curves

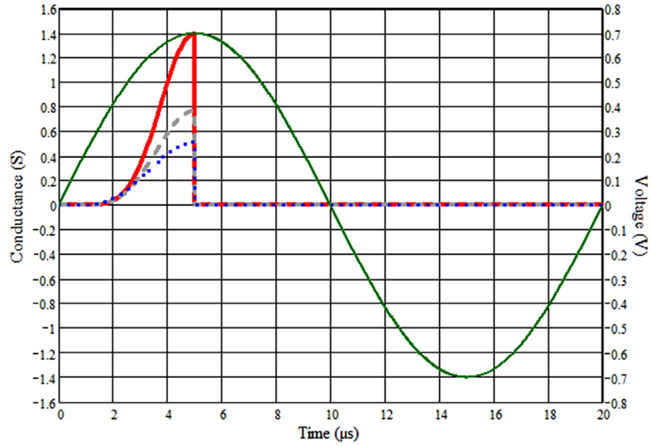

FIGURE 8 Input voltage (green) and time-variant conductance for the switched diodes D3 (red), D4 (grey) and D6 (blue)

2.5 | Time-variant resistance model of the switched diodes

The circuit of Figure 1 was simulated, using the values of the remaining parameters shown in Table 2. The simulated diode resistances in reverse bias are given by $R_{reverse}$ which was calculated using the reverse current and the specific reverse voltage stated on the diodes datasheets. The manufacturer states typical reverse bias currents of 0.05 μA at 350 V for D3, 0.05 μA at 430 V for D4 and 0.05 μA at 600 V for D3. The resulting reverse bias resistances as well as the resistance of any of the switches is R_{on} on their closed state, and R_{off} on their open state are as shown in Table 2. The selected switching frequency is 100 kHz (f_{sw}), double of the simulated input frequency of 50 kHz (f_s).

Even though the resistance of a diode is conventionally modelled in the time plane as voltage dependent, according to its *I–V*, in the Haar plane, it is easier to model as a time-variant resistance. Knowing the voltage at a diode's terminals at each time point enables the creation of a vector similar to the one shown in Ref. [12] that gives the resistance at each time point. The time-variant conductance of each switched diode (diode in series with switch as shown in Figure 1) and the source voltage for one period of f_s are shown in Figure 8.

The conductance is shown instead of resistance, in order to demonstrate the forward bias characteristics of the diode, when the diode is conducting significant current. For example, even though both for t = 0–5 and 10–15 μs, the switch which is series with a diode is on, the source voltage is not the same. This results in a different scheme. At t = 0–10 μs, the diode is in forward bias, whereas at 10–20 μs, the diode is in reverse bias. When the switch is off, a voltage divider principle distributes the voltage between the switch and the diode. For t = 15–20 μs, the division is simple as both switch and diode act as constant resistances. For t = 5–10 μs, however, the calculation is not so trivial; as the source voltage is positive, even though the switch is off, it still has a resistance value (R_{off}) and thus the voltage division has to be made between this and the non-linear resistance of the diode. This case is typically handled in the time plane graphically or by numerical iterative process using the concept of a load line as presented in Ref. [23]. Nevertheless, as the diode current would be negligible when the switch is off, this considerate difficulty can be effectively circumvented. The maximum current and thus the minimum diode resistance for the time frame of $\boldsymbol{t} = 5$–$10\ \mu$s will be for $\boldsymbol{t} = 5\ \mu$s, when $\boldsymbol{V}$ is at its peak +0.7 V. Using the load line method [23] for D3, D4 and D6, the respective currents at $\boldsymbol{t} = 5\ \mu$s are 0.68, 0.69 and 0.70 pA, respectively, and their respective resistances are 28.5, 15.6 and 4.66 GΩ. As these values represent the highest current for $\boldsymbol{t} = 5$–$10\ \mu$s, they were used as an approximation for this time length. The simulated scheme described earlier is repeated periodically every 20 μs until the end of the simulation time $\tau = 80\ \mu$s.

2.6 | Simulation method

Each of these continuous time switched diode resistance curves ($R_{D3.switched}$, $R_{D4.switched}$, $R_{D6.switched}$), the inverse of which is shown in Figure 8, was sampled, using 1024 equally distanced time points for the time length τ, and vectorised, similar to how time was vectorised in Equation (6). The vectorised input voltage ($\boldsymbol{V}$) was transformed using Equation (5) into the Haar plane vector $\boldsymbol{V}_H$. The vectorised time plane switched diode resistances ($\boldsymbol{r}_{3.switched}$, $\boldsymbol{r}_{4.switched}$, $\boldsymbol{r}_{6.switched}$) were transformed into Haar plane resistance matrices (R_{H3}, R_{H4}, R_{H6}) by using Equation (14). The impedance of the braking resistor was transformed into the Haar plane impedance matrix Z_{Hb} using Equation (11) for its resistance and Equation (8) for its inductance resulting in the following equation:

$$Z_{Hb} = r_b \cdot I_m + S \cdot L_b. \tag{16}$$

The two latter matrices R_H and Z_{Hb} were combined as the loads are in parallel, into a total Haar plane impedance matrix (Z_H), using the following equation:

$$Z_H = \left(R_H{}^{-1} + Z_{Hb}{}^{-1}\right)^{-1}. \tag{17}$$

The source current was calculated in the Haar plane in a current vector ($\boldsymbol{I_H}$) using the following equation:

$$I_H = \left(\frac{V_H{}^T}{Z_H}\right)^T. \tag{18}$$

The final step was to apply the inverse Haar transform to the Haar plane current vectors $\boldsymbol{I_{H3}}$, $\boldsymbol{I_{H4}}$ and $\boldsymbol{I_{H6}}$, respectively, using Equation (6). The result is the time plane current vectors $\boldsymbol{I_{3tot}}$, $\boldsymbol{I_{4tot}}$ and $\boldsymbol{I_{6tot}}$, as shown in Figure 9.

Equations (16)–(18), even though in the Haar plane, were presented in a manner as to resemble their Laplace-plane equivalents. For Equation (16), it would be exactly the same if I_m was replaced with 1, and S was replaced with the Laplacian variable s. Moreover, Equation (17) is identical to the one that would be used in the Laplace plane if two impedances were placed in parallel. Finally, Equation (18) is essentially an expression of Ohm's law which, if Z_H was an impedance, would similarly apply in the Laplace plane too, calculating current as voltage divided by impedance.

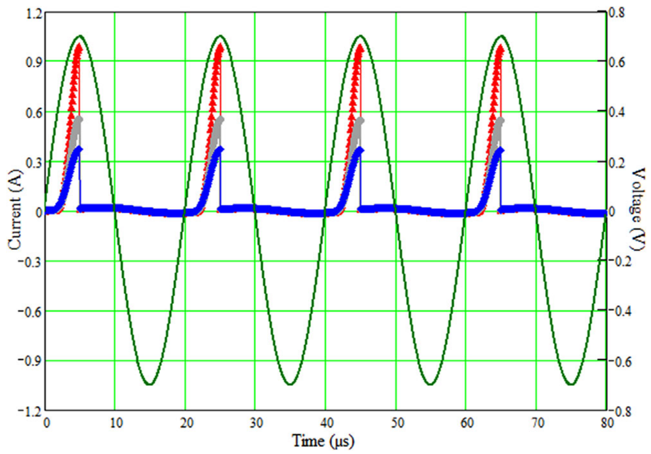

FIGURE 9 Input voltage (green) and source current for the three cases of the switched diodes D3 (red), D4 (grey) and D6 (blue) in parallel with the braking resistor

3 | RESULTS

3.1 | Simulated currents

Assuming that the inductor is not charged at $t = 0$ s and that the input voltage is 0 V for $t < 0$ s, for $N = 1024$ and $\tau = 80\ \mu$s (four periods of the input signal), all signals are presented in Figure 9.

Zooming in on the source current in the case of D6 between 20 and −20 mA, as shown in Figure 11, it is apparent that this sinusoidal response occurs due to the impedance of the braking resistor when the switched diode is switched on and in reverse bias or switched off. Its transient nature exists due to the inductance of the braking resistor. The source voltage and all currents were zero for $t < 0$ s in the simulation. This instantaneous start of the sinusoidal input is naturally followed by a transient behaviour of the inductive current, until a new steady state is reached. A full period of the source signal has to pass before its steady-state (I_s) peak current is reached as indicated in Figure 11.

3.2 | Comparison of the simulation to conventional methods

For comparison purposes as the loads are in parallel, the two currents can be separately calculated and then added. The current of D6 is directly calculated in the time plane. For the current of the braking resistor, the Laplace transform is used, in order to handle its complex-valued impedance; the current is calculated in the Laplace plane as voltage (Laplace transform of the

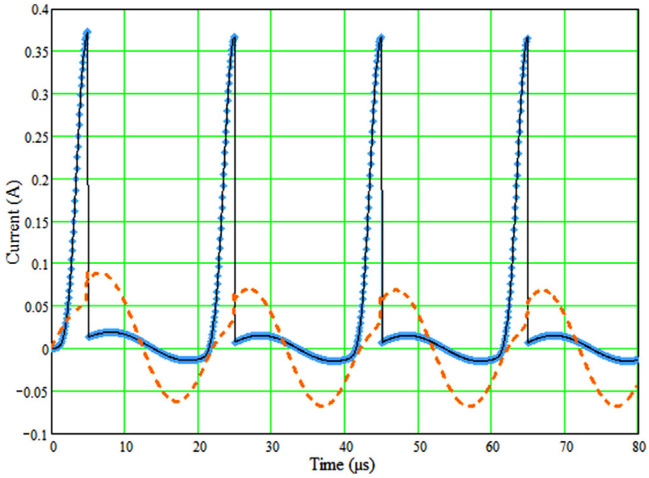

FIGURE 10 Source current for the case of the braking resistor in parallel with the switched diode D6 (blue). Calculation using the conventional method is also depicted (black). Their difference (orange) is magnified here by a factor of 10^5 for scaling purposes

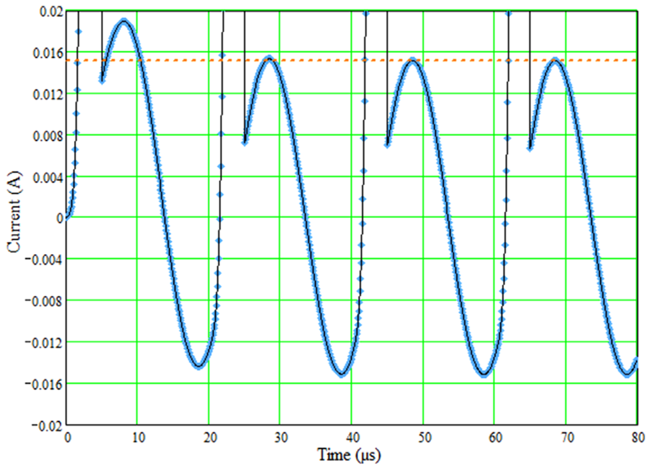

FIGURE 11 Source current for the case of the braking resistor in parallel with the switched diode D6 (blue). A transient response, related to the inductance of the braking resistor, is evident as its steady-state peak I_s (orange) is gradually reached. For comparison, calculation using the conventional method is also depicted (black)

input voltage) divided by impedance, similar to Equation (18). Then, the inverse Laplace transform of this current is the current of the braking resistor in the time plane. The results shown in Figure 10 and more focused in Figure 11 depict the conformity of the Haar transform to the conventional methods. A detailed analysis on the accuracy of the Haar wavelet discretisation method theoretically can be found in Ref. [24]. It is noted that one of the main reasons why the circuit of Figure 1 was selected to be simulated was its ability to be simulated both via the conventional methods and in the way of the presented method. The source being in parallel with the linear and the non-linear, time-variant components enabled separating their calculations in the time and Laplace plane, respectively. For a more advanced circuit, for example having a source impedance, it would have been impossible by definition to handle it conventionally and thus compare between this and the conventional method: The voltage drop across the source impedance would be a result of the total source current, which in its turn would depend both on linear and non-linear, time-variant components, rendering handling either in the time or Laplace plane impossible.

Comparing between the conventional and the presented method for D6 is performed by calculating the difference d for the source current by Equation (19). It is noted that the conventional method gives an exact value (i_{exact}) in comparison to the presented method that is a numerical approximation ($i_{approximated}$). As shown in Figure 10, the difference between the approximation and the exact values is remarkably low. Specifically, the absolute error (absolute of $\boldsymbol{d}$) has a maximum value of 899 nA, a mean of 436 nA and a median of 481 nA. In comparison between signal and error, the absolute of the maximum of the source current is more than five orders of magnitude higher, having a maximum of 377 mA, which compared to the maximum of the absolute error, reveals a ratio of 415,056/1. These remarkable error margins depict the closely simulated character that is shown in Figures 10 and 11:

$$d = i_{approximated} - i_{exact}. \tag{19}$$

It is also noted that the relative errors or per cent errors were not used as indicators in the error evaluation, because diving the absolute error with the zero-crossing values of i_{exact} would cause very high relative and per cent error values around very small current values, which is not representative of the accuracy of the method. For example on a hypothetical sinusoidal current signal of 0.4 A amplitude, a 100% error could mean an approximation value of 2 pA instead of the exact 1 pA; if the same signal had an error below 0.1% for all values except from −1 to 1 nA, the aforementioned 100% error would be misleading in that context.

4 | DISCUSSION

4.1 | Overview

Impedance measurements on linear loads and *I*–*V* measurements on diodes were performed and then fitted. The *I*–*V* fittings used were only indicative and any straight-forward interpolation between measurement points could also have been applied in the case of non-linear loads because, as stated in Section 2.1, Equation (14) can also be used to approximate the resistance of a non-linear component. The resistance can consequently be automatically (by a fitting model) or manually defined at each time point.

Three versions of a circuit consisting of a voltage source in parallel with a linear impedance and a switched diode were compared, using three different diodes. The diversity of the potential uses of the Haar wavelet as an analysis tool of non-linear, time-variant systems was demonstrated; linear impedance as well as non-linear, time-variant loads were evidently handled. The key step where linear and non-linear, time-variant loads were ultimately combined was in Equation (17), notably before applying the inverse Haar transform. The source current features are depicted in Figures 9 and 11. This method of using the Haar wavelet transform was shown to be in agreement with the conventional methods in Section 3.2, as the calculated points accurately follow the continuous curves, as depicted in Figures 10 and 11. The difference of the approximation from the exact values is remarkably low, as shown in Section 3.2 and depicted in Figure 10, showcasing the capabilities of this method as an accurate tool for circuit simulation.

4.2 | Advantages of the method

The usefulness and simplicity of this approach in load modelling were showcased as linear, non-linear and time-variant components can thus be transformed using the same principles as the widely known Laplace transform, as shown in Equations (16)–(18).

The intricacy of a forward and inverse Laplace transform of a non-linear, time-variant system is effectively circumvented. The reason is that both the Haar forward and inverse transform are performed by a simple multiplication as shown in Equations (5) and (6).

Furthermore, it is presented in a step-by-step approach, how starting with direct measurements on components, a complete numerical simulation of circuits using these components can be obtained.

The Haar wavelet operational matrix is used multiple times applying Equation (5) or (6) but it only needs to be calculated or loaded once. This results in reducing significantly the total calculation time, as the matrix is readily used in simple multiplications without being calculated again each time.

4.3 | Further considerations

It is noted that the choices of f_s and f_{sw} are based on three factors. First, it had to be in the measurable range of the LCR instrument. Second, it had to demonstrate a transient response as shown in Figure 11. Third, for f_{sw}, an integer multiple (double) of the simulated input frequency f_s was chosen, in order for the transient effects from period to period to be comparable, as shown in Figure 11. This way, every 5 μs, the state of the switch which is in series with each diode and alternates between on and off can be exactly compared for different input voltage states.

4.4 | Importance of the *I*–*V* measurements and custom models

Comparing between measurements and datasheets for the three diodes, the expected currents at 0.7 V varied significantly. According to their datasheets, the currents at 0.7 V should be 0.8, 0.3 and 0.3 A, respectively, at room temperature (25°C) and 2.0, 1.0 and 0.8 A for a temperature of 75°C. The measured currents at this voltage were instead 0.98, 0.54 and 0.36 A at a room temperature of approximately 21°C.

This considerable difference between what was expected and what was measured could have been due to internal elevated temperature, even though the time needed for this measurement was only 1 s approximately, and a heat sink was attached to the diodes. It is noted that the internal temperature would have to be much higher than room temperature, and no indication of such a phenomenon was observed on the package of the diodes during the measurement. Another cause, even though not explicitly stated in the diodes datasheets, could be the tolerance of the characteristics of the diodes.

The concept of creating custom models and its application via the Haar wavelet transform is emphasised as it can greatly improve the accuracy of a simulated scenario. For example, a resistor of nominal value 10 Ω and 10% tolerance will by definition have an actual value between 9 and 11 Ω. Accurately measuring and determining its resistance at for example 9.23 Ω would significantly increase the accuracy and precision of the simulated component as opposed to using its nominal value of 10 Ω. The same principle can be extended to any property or characteristic of a simulated component as tolerances, even though not always stated, intrinsically exist. Other factors such as temperature may also affect the behaviour of any component, and thus measuring the component at parameters (e.g. voltage and current) and conditions (e.g. room temperature) as close to the ones desired to simulate is significantly valuable in order to predict the expected circuit performance and possibly avoid a faulty operation. This can be better achieved by performing measurements on the respective components before placing them in the final circuit. It is noted that even though some parameters may not be accurately known (e.g. core component temperature at a high DC current), by using the same or similar parameters as in the simulation (e.g. use same peak voltage or current at the actual diode *I*–*V* measurement as it will be in the simulated circuit), a higher level of accuracy can be obtained.

4.5 | Suitable potential applications of the Haar wavelet transform

Utilising most of the already widely used techniques of Fourier and Laplace transforms, the Haar wavelet transform has great potential for use in a wide scientific and engineering spectrum. Combining this aspect with the addition of non-linear, time-variant elements, scientific instruments and devices could considerably benefit. Some examples are network analysers, digital signal processors and automated control systems, which could potentially use it to solve non-linear equations previously impossible.

Finally, this work aspires to be an additional step towards popularising wavelet theory and particularly the Haar wavelet transform. Its intrinsic useful properties and key applications could thus in the future be more integrated into various sectors of higher education (at e.g. B.Sc. or M.Sc. level). Sectors such as mathematics, physics, chemistry, materials science, civil and electrical engineering are highly suitable for applications of this method, as they frequently handle differential and non-linear equations, trying to depict the true nature of signals and systems.

5 | CONCLUSION

The Haar wavelet has already proven that it can efficiently handle solving non-linear and differential equations [2, 25–34] and is frequently applied in simple circuits and systems [35–45], so all that remains is that proper applications and methods are established. An example of circuit simulation method using the Haar wavelet was demonstrated and evaluated. Custom device models were created using direct measurements. The intricacies of this simulation method for the output of a system that includes linear (resistances), reactive linear (inductances), but also non-linear (diodes) and time-variant (switches), components, were discussed. The approximation error as compared to the exact output of signal amplitude was found to be more than five orders of magnitude lower, that is in terms of comparing the maximum of the absolute of the output signal to the maximum of the absolute error of its approximation. This level of accuracy is indicative of the potential of the simulation method in circuits when calculating integrals for the convolution of all signals and components of a circuit results in impractical simulation times.

ACKNOWLEDGEMENTS

The authors would like to thank the B.Sc. student Michiel Reyntjens for manufacturing the circuit used to obtain the diodes I–V measurements. This work is part of and funded by the BOF project 01N15419.

CONFLICT OF INTEREST

The authors declare that there is no conflict of interest that could be perceived as prejudicing the impartiality of the research reported.

FUNDING INFORMATION

This work is part of and funded by the BOF project 01N15419.

DATA AVAILABILITY STATEMENT

The data that support the findings of this study are available from the corresponding author upon reasonable request.

REFERENCES

1. Heideman, M.T., Johnson, D., Burrus, C.: Gauss and the history of the fast Fourier transform. IEEE ASSP Mag. 1(4), 265–274 (1985). https://doi.org/10.1109/massp.1984.1162257
2. Chen, C.F., Hsiao, C.H.: Haar wavelet method for solving lumped and distributed-parameter systems. IEE Proc. Control Theory Appl. 144(1), 87–94 (1997). https://doi.org/10.1049/ip-cta:19970702
3. Jain, A., Pankanti, S.: Chapter 8: Automated fingerprint identification and imaging systems. In: Advances in Fingerprint Technology, pp. 283. CRC Press, Boca Raton, FL, USA (2001). https://doi.org/10.1201/9781420041347.ch8
4. Wu, J.L., Chen, C.H., Chen, C.F.: Numerical inversion of Laplace transform using Haar wavelet operational matrices. IEEE Trans. Circuits Syst. I: Fundam. Theory Appl. 48, 120–122 (2001). https://doi.org/10.1109/81.903196
5. Aznam, S.M., Hussin, A.: Numerical method for inverse Laplace transform with Haar wavelet operational matrix. Malays. J. Fundam. Appl. Sci. 8(4), 204–210 (2012). https://doi.org/10.11113/mjfas.v8n4.149
6. Ohkubo, A., Moro, S., Matsumoto, T.: A method for circuit analysis using Haar wavelet transform. Presented at the 2004 47th Midwest symposium on circuits and systems. (July 2004). MWSCAS '04. [Online]. Available: https://doi.org/10.1109/MWSCAS.2004.1354379
7. Nakabayashi, T., Mochizuki, M., Moro, S.: Analysis method of periodic solution using Haar wavelet transform for autonomous nonlinear circuits. Presented at 2015 international symposium on intelligent signal processing and communication systems (ISPACS). (2015). [Online]. Available: https://doi.org/10.1109/ispacs.2015.7432775
8. Sliwinski, P.: Chapter 1: Introduction. In: Nonlinear System Identification by Haar Wavelets, pp. 1–4. Springer-Verlag Berlin Heidelberg, Wrocław, Poland (2013). https://doi.org/10.1007/978-3-642-29396-2
9. Hsiao, C.H., Wang, W.J.: State analysis of time-varying singular nonlinear systems via Haar wavelets. Math. Comput. Simul. 51(1–2), 91–99 (1999). https://doi.org/10.1016/s0378-4754(99)00107-x
10. Hsiao, C.H., Wang, W.J.: State analysis and optimal control of linear time-varying systems via Haar wavelets. Optim. Control Appl. Methods 19(6), 423–432 (1998). https://doi.org/10.1002/(SICI)1099-1514(199811/12)19:6<423::AID-OCA638>3.0.CO;2-G
11. Hsiao, C.H., Wang, W.J.: Optimal control of linear time-varying systems via Haar wavelets. J. Optim. Theory Appl. 103(3), 641–655 (1999). https://doi.org/10.1023/a:1021740209084
12. Zhou, D., Li, X., Zhang, W., Cai, W.: Nonlinear circuit simulation based on adaptive wavelet method. Presented at 1997 IEEE international symposium on circuits and systems (ISCAS). (1997). [Online]. Available: https://doi.org/10.1109/iscas.1997.621471
13. Zhou, D., Chen, N., Cai, W.: A fast wavelet collocation method for high-speed VLSI circuit simulation. In: Proc. of IEEE International Conference on Computer Aided Design (ICCAD), San Jose, CA, USA, pp. 115–122 (1995) https://doi.org/10.1109/iccad.1995.480001
14. Cheng, C.F., Tsay, Y.T., Wu, T.T.: Walsh operational matrices for fractional calculus and their application to distributed systems. J. Franklin Inst. 303(3), 267–284 (1977). https://doi.org/10.1016/0016-0032(77)90029-1
15. Strang, G.: Wavelet transforms versus Fourier transforms. Bull. Am. Math. Soc. 28(2), 288–303 (1993). https://doi.org/10.1090/s0273-0979-1993-00390-2
16. Souza, D., Barbosa, U., Guido, R.C., da Silva, I.N.: The Haar Wavelet transform in IoT digital audio signal processing. Circuits Syst. Signal Process. 1, pp. 1–11, Cham, Switzerland (2022). https://doi.org/10.1007/s00034-022-01979-8
17. Cheng, Y., Zhang, X., Wang, X., Li, J.: Battery state of charge estimation based on composite multiscale wavelet transform. Energies 15(6), 1–16 (2022). https://doi.org/10.3390/en15062064
18. Ge, X., Xie, Y., Chen, Y., Liang, T.: Uncertainty quantification of self-breakdown switches in a circuit model using Wiener–Haar expansion. IEEE Trans. Electromagn. Compat. 64, 27–32 (2021). https://doi.org/10.1109/TEMC.2021.3087200
19. Kumar, A.N., Sitharamaiah, N., Chakravarthy, M.: Series capacitor-compensated double-circuit transmission line directional relay system using a fuzzy expert system with a Haar wavelet. Iran J. Comput. Sci. 5, 157–166 (2022). https://doi.org/10.1007/s42044-021-00097-z
20. Pant, S., Nema, R.K., Gupta, S.: Detecting faults in power transformers using wavelet transform. In: IEEE ICEPES, pp. 1–5 (2021). https://doi.org/10.1109/ICEPES52894.2021.9699483
21. Ratas, M., Majak, J., Salupere, A.: Solving nonlinear boundary value problems using the higher order Haar wavelet method. MDPI Math. 9(21), 1–12 (2021). https://doi.org/10.3390/math9212809
22. Akujuobi, C.M.: Wavelets and Wavelet Transform Systems and Their Applications. Springer, Cham, Switzerland (2022). https://doi.org/10.1007/978-3-030-87528-2
23. Sedra, A.S., Smith, K.C., Tony, C.C., Gaudet, V.: Diodes. In: Microelectronic Circuits, vol. 4, pp. 191–192. Oxford University Press, New York (2004)

24. Majak, J., Shvartsman, B., Karjust, K., Mikola, M., Haavajõe, A., Pohlak, M.: On the accuracy of the Haar wavelet discretization method. Composites, B: Eng. 80, 321–326 (2015), https://doi.org/10.1016/j.compositesb.2015.06.008
25. Aznam, S.M., Ghani, N.A.C., Chowdhury, M.S.H.: A numerical solution for nonlinear heat transfer of fin problems using the Haar wavelet quasilinearization method. Results Phys. 14(102393), 1–7 (2019). https://doi.org/10.1016/j.rinp.2019.102393
26. Aznam, S.M., Chowdhury, M.S.H.: Generalized Haar wavelet operational matrix method for solving hyperbolic heat conduction in thin surface layers. Results Phys. 11, 243–251 (2018). https://doi.org/10.1016/j.rinp.2018.08.021
27. Takamatsu, K., Nakabayashi, T., Moro, S.: Analysis of unstable periodic solution of nonlinear circuits using Haar wavelet transform. Presented at 2016 international symposium on intelligent signal processing and communication systems (ISPACS). (2016). [Online]. Available: https://doi.org/10.1109/ispacs.2016.7824737
28. Swaidan, W., Hussin, A.: Haar wavelet operational matrix method for solving constrained nonlinear quadratic optimal control problem. AIP Conf. Proc. 1682(1), 020004 (2015). https://doi.org/10.1063/1.4932413
29. Hariharan, G., Rajaraman, R., Kannan, K.: Haar wavelets approach of traveling wave equation—a plausible solution of lightning stroke model. Int. J. Eng. Technol. 2(2), 149–156 (2013). https://doi.org/10.14419/ijet.v2i2.869
30. Ray, S.S., Patra, A.: Haar wavelet operational methods for the numerical solutions of fractional order nonlinear oscillatory Van der Pol system. Appl. Math. Comput. 220, 659–667 (2013), https://doi.org/10.1016/j.amc.2013.07.036
31. Swaidan, W., Hussin, A.: Feedback control method using Haar wavelet operational matrices for solving optimal control problems. Abstr. Appl. Anal. 2013, 1–7 (2013). https://doi.org/10.1155/2013/240352
32. Shi, Z., Deng, L.Y., Chen, Q.J.: Numerical solution of differential equations by using Haar wavelets. Presented at 2007 international conference on wavelet analysis and pattern recognition. (2007). [Online]. Available: https://doi.org/10.1109/icwapr.2007.4421585
33. Lepik, Ü.: Application of the Haar wavelet transform to solving integral and differential equations. Proc. Est. Acad. Sci. Phys. Math. 56(1), 28–44 (2007). https://doi.org/10.1117/12.736416
34. Lepik, Ü.: Numerical solution of differential equations using Haar wavelets. Math. Comput. Simul. 68(2), 127–141 (2005). https://doi.org/10.1016/j.matcom.2004.10.005
35. Abuhamdia, T., Taheri, S.: Wavelets as a tool for systems analysis and control. J. Vib. Control 23(9), 1–36 (2015). https://doi.org/10.1177/1077546315620923
36. Daza, R.J.M., Ruiz, C.P., Aguilar, L.J.: Two-dimensional fast Haar wavelet transform for satellite-image fusion. J. Appl. Remote Sens. 7(1), 1–13 (2013). https://doi.org/10.1117/1.jrs.7.073698
37. Moro, S., Shoji, T.: Error evaluation of circuit analysis method using Haar wavelet transform. Presented at 2011 20th European conference on circuit theory and design (ECCTD). (2011). [Online]. Available: https://doi.org/10.1109/ecctd.2011.6043382
38. Oishi, M., Moro, S., Matsumoto, T.: A modified method for circuit analysis using Haar wavelet transform with adaptive resolution—for circuits with waveform with sharp convex ranges. Presented at 2009 European conference on circuit theory and design. August (2009). [Online]. Available: https://doi.org/10.1109/ecctd.2009.5274922
39. Zhi-yong, Y., Hua-long, X., Guang-bin, L.: Transient analysis of unequal length multiconductor transmission lines via Haar wavelets-based numerical inversion of Laplace transform. In: Asia-Pacific Conf. on Environmental Electromagnetics CEEM 2003: Proc., Hangzhou, China, pp. 260–263 (2003). https://doi.org/10.1109/ceem.2003.237960
40. Falkowski, B.J., Stankovic, R.S., Jankovic, D.: Circuit design from minimized Haar wavelet series. In: 2002 IEEE International Symposium on Circuits and Systems. Proc. (Cat. No. 02CH37353), Phoenix-Scottsdale, AZ, USA, vol. 3, pp. 381–384, (2002). https://doi.org/10.1109/iscas.2002.1010240
41. Gandelli, A., Monti, A., Ponci, F.: Time evolution of Haar spectra for periodic switching circuits, 2000. In: IEEE 31st Annual Power Electronics Specialists Conf. Conf. Proc. (Cat. No. 00CH37018), Galway, Ireland, vol. 1, pp. 280–285. (2000). https://doi.org/10.1109/pesc.2000.878858
42. Hsiao, C.H.: State analysis of linear time delayed systems via Haar wavelets. Math. Comput. Simul. 44(5), 457–470 (1997). https://doi.org/10.1016/s0378-4754(97)00075-x
43. Chacon-Rodriguez, A., Li, S., Stanaćević, M., Rivas, L., Baradin, E., Julian, P.: Low power switched capacitor implementation of discrete Haar wavelet transform. Presented at 2012 IEEE 3rd Latin American symposium on circuits and systems (LASCAS). (2012). [Online]. Available: https://doi.org/10.1109/lascas.2012.6180333
44. Abdeljawad, T., Amin, R., Shah, K., Al-Mdallal, Q., Jarad, F.: Efficient sustainable algorithm for numerical solutions of systems of fractional order differential equations by Haar wavelet collocation method. Alex. Eng. J. 59(4), 2391–2399 (2020). https://doi.org/10.1016/j.aej.2020.02.035
45. Li, C., Yu, Y., Yang, Z., Liu, Q., Peng, X.: ESR Estimation for aluminum electrolytic capacitor of power electronic converter based on compressed sensing and wavelet transform. IEEE Trans. Ind. Electron. 69(2), 1948–1956 (2021). https://doi.org/10.1109/TIE.2021.3055164

How to cite this article: Roumeliotis, G.G., Desmet, J., Knockaert, J.: Simulation of a non-linear, time-variant circuit using the Haar wavelet transform. IET Sci. Meas. Technol. 16, 389–399 (2022). https://doi.org/10.1049/smt2.12112